VIP Solid-State Chemistry Very Important Paper

How to cite: *Angew. Chem. Int. Ed.* **2023,** *62,* e202215544
International Edition: doi.org/10.1002/anie.202215544
German Edition: doi.org/10.1002/ange.202215544

Frustration in Super-Ionic Conductors Unraveled by the Density of Atomistic States

*Shuo Wang, Yunsheng Liu, and Yifei Mo**

Abstract: The frustration in super-ionic conductors enables their exceptionally high ionic conductivities, which are desired for many technological applications including batteries and fuel cells. A key challenge in the study of frustration is the difficulties in analyzing a large number of disordered atomistic configurations. Using lithium super-ionic conductors as model systems, we propose and demonstrate the density of atomistic states (DOAS) analytics to quantitatively characterize the onset and degree of disordering, reveal the energetics of local disorder, and elucidate how the frustration enhances diffusion through the broadening and overlapping of the energy levels of atomistic states. Furthermore, material design strategies aided by the DOAS are devised and demonstrated for new super-ionic conductors. The DOAS is generally applicable analytics for unraveling fundamental mechanisms in complex atomistic systems and guiding material design.

Introduction

Frustration is a physical phenomenon widely existing in magnetism,[1] spin lattice,[2] water ice,[3] and quantum many-body systems,[4] in which a plenitude of competing states exist with similar energy levels. The frustration of the mobile-ion sublattice in a solid makes a super-ionic conductor (SIC), a type of material exhibiting exceptionally high ionic conductivities compared to typical solids. SICs are of great technological importance as solid electrolytes or electrodes for batteries, fuel cells, and novel electrochemical devices.[5] In particular, Lithium SICs such as $Li_{10}GeP_2S_{12}$,[5b] $Li_7P_3S_{11}$,[6] argyrodite Li_6PS_5X (X = Cl, Br, I),[7] NASICON-type $Li_{1.3}Al_{0.3}Ti_{1.7}(PO_4)_3$,[8] lithium-garnet $Li_7La_3Zr_2O_{12}$,[9] with high ionic conductivities of $>1\,mS\,cm^{-1}$ at room temperature, are the key materials to enable the next-generation all-solid-state lithium batteries.

An SIC features a disordered mobile-ion sublattice with partial site occupancy, allowing a large fraction of ions to migrate with low energy barriers. By contrast, a typical solid exhibits a mobile-ion sublattice "locked" in its ground-state, ordered configurations, hence giving poor ion conduction. A super-ionic transition (SIT) turns a material into a SIC above the critical temperature T_c, through the disordering of the mobile-ion sublattice. The disordered mobile-ion sublattice has a large number of distinctive ion configurations in the crystal structure with similar energies, which can be understood by the frustration mechanism.[10] Having a large number of possible configurations within a close range of energy levels allows many possible transitions among them, which correspond to ion hopping in the crystal lattice. Those transitions with lower energy barriers are predominantly activated, giving an overall low activation energy for ion conduction in SICs.[10a,g,11]

A key strategy of designing SIC materials is to lower T_c by enabling the frustration of mobile-ion sublattices over a wide temperature range. To achieve this, it is critical to understand the frustration mechanisms of ion sublattice during SIT. A number of frustration mechanisms caused by distorted sites, sublattice symmetry, mixed ionic-covalent bonding, and poly-anion rotation, which can be described by specific descriptors, such as the geometry of mobile-ion sites, symmetry groups, local bond characters, and collective ion motions, respectively, are identified by computation studies in a range of SIC materials.[10] Besides these descriptors, unified quantitative measures and characterization of frustration mechanisms across different SIC materials are still lacking, impeding the capability to design new SIC materials.

The computation analytics for the frustration is urgently needed at the fundamental level, that is, quantifying, evaluating, and assessing a large number of atom configurations and their corresponding energy levels in a disordered lattice. Such computation analytics would be helpful in quantitatively elucidating and characterizing the onset and the degree of frustration in SICs and during SIT. Furthermore, these analytics can also help answer scientific questions for understanding the frustration in SICs. For example, the study of SICs often deals with questions regarding how frustration and disordering change local atomic configurations and energetics. Another important scientific question is how the ion diffusion mechanisms are

[*] S. Wang, Y. Liu, Y. Mo
Department of Materials Science and Engineering
University of Maryland
College Park, MD 20742 (USA)
E-mail: yfmo@umd.edu
Y. Mo
Maryland Energy Innovation Institute, University of Maryland
College Park, MD 20742 (USA)

changed in a disordered mobile-ion sublattice of a SIC and how the energy barriers are lowered under frustration.

To answer these questions across different SIC materials, quantitative analytics from atomistic modeling that can be generally applicable is essential. However, a long-standing challenge is that analyzing a large number of disordered configurations of the atomistic systems and their energies using first principles computation is computationally expensive. Here, with the aid of machine learning interatomic potential (MLP)[12] to accelerate atomistic modeling and to provide atomistic energies of individual atoms,[13] we propose the density of atomistic states (DOAS) for quantitatively analyzing, elucidating, and characterizing the energetics for a large number of atomic states with disordered configurations in frustrated materials. The DOAS is demonstrated as highly effective analytics in unraveling the frustration mechanisms during the SIT in the SICs, and is further employed in guiding the rational design of new SIC materials.

Results and Discussion

Frustration through super-ionic transition

We study the SIT in the model system Li_3YCl_6 (LYC), which is a Li-ion conductor with both high ionic conductivity and good electrochemical stability for solid-state batteries.[14] The LYC has a $P\bar{3}m1$ trigonal lattice composed of hexagonal close-packed (hcp) Cl^- sublattice with alternating Y-rich and Y-poor layers in which Y^{3+} and Li^+ occupy the octahedral (Oct) sites (Figure 1d). A machine-learning interatomic potential (MLP) using the Deep Potential (DP) formalism[12a] is trained through the active learning scheme implemented in the DP-GEN package[15] (Methods). The trained DP MLP accurately reproduces the energies, atomic forces, and lattice parameters, in agreement with density functional theory (DFT) calculations (Figure S1 and Table S4). Thanks to its lower computation cost, the MLP significantly extends the time scale of the MD simulations, and thus enables the observation of a large number of diffusional events in MD simulations at lower temperatures,[16] leading to accurate quantification of Li^+ conductivities in agreement with experiments.[17] An SIT is observed at a T_c of 425 K in the Arrhenius plot of Li^+ conductivity (Figure 1a), in agreement with MD simulations in Ref. [18]. Below T_c, the extrapolated σ_{RT} is 0.02 mS cm^{-1}, in good agreement with the experimental value of 0.01 mS cm^{-1} for LYC with high crystallinity.[14b,17] The ordered Li^+ sublattice below T_c has Li ions occupying only octahedral Li (Oct-Li) sites (Figure 1d), consistent with the structures from neutron powder diffraction refinement.[14b] During the SIT, the crystal structure framework of Cl^- and Y^{3+} remains the same (Figure 1c and d), and the only change is the order-disorder transition of the Li^+ sublattice. Above the T_c of 425 K, the disordered Li^+ sublattice is confirmed by the peak broadening of the Li radial distribution function (RDF) (Figure S3), and exhibits partial occupancies in Oct-Li and tetrahedral Li (Tet-Li) sites (Figure 1c). The LYC is a SIC exhibiting a low activation energy of 0.24 eV in agreement with the AIMD simulations[14a] (Figure S2).

Frustration characterized by the DOAS

The DOAS of Li-ions is proposed and demonstrated to quantitatively elucidate and characterize the SIT and frustration in the LYC SIC, in particular, the atom configurations and their corresponding energy levels of the mobile-ion sublattice (Figure 2 and S4). The Li DOAS is calculated as a histogram of atomistic energies of the Li-ion states. Each Li-ion state corresponds to a distinct local configuration of a Li-ion with different configurations of surrounding cations and vacant sites (Figure 2), and its atomistic energy is obtained from the MLPs. The Li DOAS is constructed by evaluating every Li-ion in the structure snapshots, which are sampled from MD simulations and are then statically relaxed to eliminate the energy fluctuations from thermal vibrations (Methods). Through this static relaxation, the effects of larger vibration magnitude around the site equilibrium positions at higher temperatures are eliminated, and the energy changes originated mostly from the different Li-ion configurations, given the non-Li sublattice remains the same.

The disordered Li^+ sublattice corresponds to a large number of ion configurations with a range of energies, as shown by the DOAS of the total energy of the Li^+ sublattice (Figure S5), confirming the frustration during the SIT. In addition, the average energy of the Li^+ sublattice shows a clear thermodynamic transition of the Li^+ sublattice at T_c (Figure S7). This transition of Li^+ sublattice coincides with the transition in the Arrhenius plots of Li^+ ionic conductivity (Figure 1). Therefore, the disordering and frustration of Li^+ sublattice are responsible for activating LYC into a SIC.

The DOAS of individual Li^+ clearly elucidates the local states of Li^+ and their energy levels (Figure 2, Figure S4). For the ordered Li^+ sublattice at low temperatures (e.g. 300 K), the Li DOAS shows two peak states, corresponding to the two Oct-Li in the Y-poor and Y-rich layers, respectively (Figure 2a). After the SIT above T_c, as shown in the Li DOAS, these two peak states broaden into a large variety of local configurations, i.e., Li-ion states, with a range of small energy differences (Figure 2b). This plenitude of Li states with small energy differences manifests the frustration of the Li^+ sublattice. The DOAS of Li-ions effectively illustrates the frustration in SICs during SIT.

In addition, as shown in Li DOAS (Figure 2b), a large number of Tet-Li states are activated after SIT, in agreement with the structures observed in MD simulations (Figure 1c). The activation of Tet-Li can be explained by the greatly reduced energy barriers between Oct- and Tet-Li states, as shown by the overlapping among broadened energy levels of Oct- and Tet-Li states (Figure 2b). In consistency with the disordered local configurations after SIT (Figure 1c), the increase of Tet-Li states, in turn, leads to a large variety of local cation configurations of Oct-Li states (Figure 2b). By contrast, the activation of Tet-Li sites

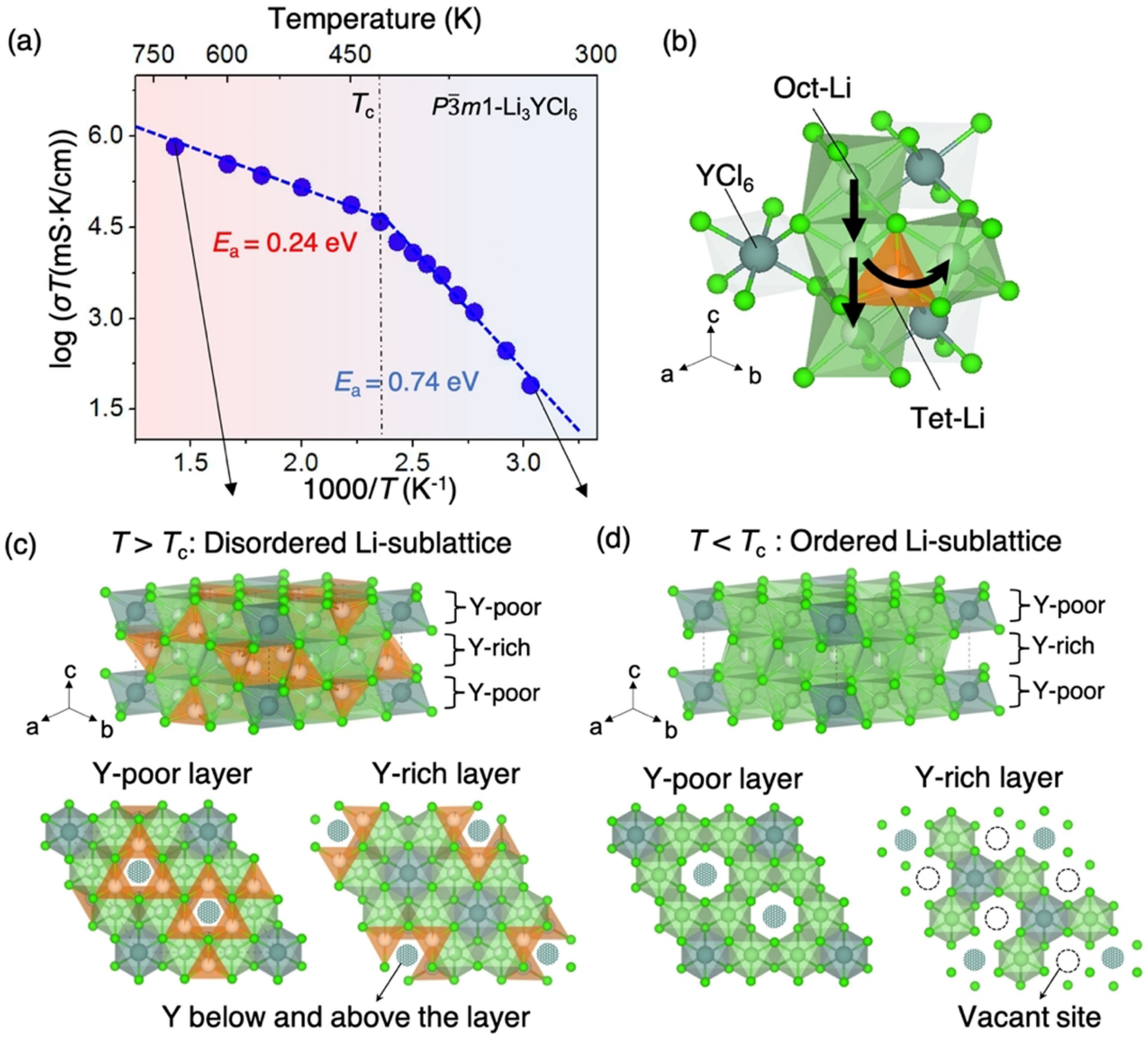

Figure 1. Super-ionic transition in Li_3YCl_6. a) Arrhenius plot of Li^+ conductivity in $P\bar{3}m1$-LYC and b) the Li-ion migration pathways in the crystal structure. c), d) The crystal structures of $P\bar{3}m1$-LYC with Oct-Li (green), Tet-Li (orange), Y (grey), and Cl (light-green), c) after and d) before the SIT, respectively. d) Below T_c, in the ordered Li^+ sublattice, Li ions occupy Oct-Li sites. c) Above T_c, the disordered Li^+ sublattice has partial occupancies in Tet-Li sites (orange) that are not face-sharing with Y.

in the ordered Li^+ sublattice is impeded by the large energy gaps between Oct- and Tet-Li states as shown in the Li DOAS (Figure 2a). In summary, the DOAS unravels how the SIT and frustration are caused by the changes of local configurations and energetics of individual atoms.

Facilitated diffusion under frustration

The mechanisms of Li-ion diffusion can also be illustrated and analyzed as the transitions among Li-states in the DOAS. The hcp Cl-anion framework of LYC has two diffusion pathways (Figure 1b), Oct-Oct channels along the *c* axis, and Oct-Tet-Oct pathways connecting Oct-Oct channels.[14a] In the ordered Li-ion sublattice below T_c, Li^+ migrations along the Oct-Oct pathways correspond to transitions between the two Oct-Li states in the Li DOAS (Figure 2a, Figure 3a), but this pathway cannot percolate without the formation of an extra Li vacancy, which has a high formation energy (Figure S8). For the Oct-Tet-Oct pathway, Li^+ migrates through intermediate Tet- and Oct-sites, shown as the small high-energy states in Li DOAS (insets in Figure 2a, and Figure 3a), and exhibits a high energy barrier of 0.46 eV calculated by nudged-elastic-band (NEB) method (Figure 3c). Therefore, in the ordered Li^+ sublattice, Li-ion migrations are impeded by the lack of

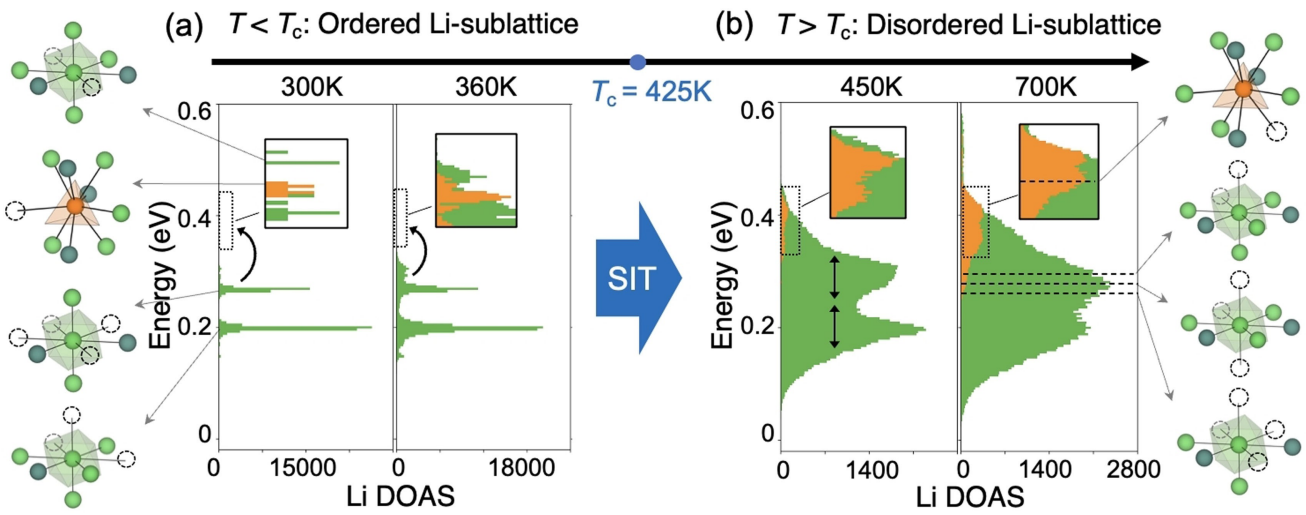

Figure 2. Frustration and SIT elucidated by the density of atomistic states (DOAS). a), b) The Li DOAS and representative local configurations of Li states with neighboring Oct-Li (green), Tet-Li (orange), Y (grey), a) before and b) after the SIT in $P\bar{3}m1$-LYC. The energy levels are referenced to the lowest-energy state among the entire range of temperatures studied.

percolation among the limited number of accessible Li-states as illustrated in Li DOAS (Figure 3a).

How does the frustration of the mobile-ion sublattice enhance ion diffusion in SICs? (Figure 3). As elucidated by the Li DOAS above T_c, disordered Li^+ sublattice has a large number of Tet- and Oct-Li states, which have many different ion configurations (Figure S16) and thus a range of broadened energy levels (Figure 2b). As a result of a large number of local Li^+ configurations, many Oct Li^+ ions have more vacant Oct-sites nearby due to the disordering and the activated occupancy of Tet-sites, thus opening many local diffusion pathways for hopping and the long-range percolation in the crystal structure, as observed in MD simulations (Figure S15). Furthermore, the transitions among these Li states, i.e., Li-ion migrations among these Li sites, have significantly lower energy barriers (Figure 3b), because the broadened energy levels for a large number of Tet- and Oct-Li states have partial overlap and reduced gaps of energy levels (Figure 2b). Li-ion migrations along Oct-Tet-Oct pathways as observed in MD simulations are calculated to have lower energy barriers of 0.03–0.25 eV (Figure 3d and S9). The Oct-Oct pathways also have low barriers of 0.08–0.24 eV thanks to the overlapping of the broadened Oct-Li states (Figure 3e and S10). Given a large number of possible ion-hopping pathways with significantly lower energy barriers, many of which are dominantly activated for ion-hopping, leading to a low overall activation energy for ion conduction. Therefore, the broadening of Li^+ states induced by the frustration reduces the energy barriers for ion diffusion, as elucidated by the Li DOAS (Figure 3b).

Design super-ionic conductors by facilitating frustration

The DOAS can guide the design of new SIC materials. New SICs can be designed by facilitating the frustration of mobile-ion sublattice specifically through 1) introducing higher-energy states or 2) broadening the states of mobile-ions (Figure 4a–c). These induced mobile-ion states have narrowed energy gaps to the activated states, thus yielding low energy barriers for ion diffusion. Here these two design strategies are demonstrated through the modification of the cation or anion sublattice in LYC.

For the SIC with modified cation sublattice, we study the *Pnma* LYC polymorph of the orthorhombic structure with identical hcp Cl-anion sublattice but a different Y-cation sublattice (Figure S13), which was synthesized by annealing LYC at 480 K.[19] As illustrated by the Li DOAS (Figure 4b), new high-energy Oct-Li states are introduced by the distinct Y^{3+} cation sublattice in the *Pnma* structure (Figure 4h and S14). The new Oct-Li states have narrowed energy gaps to Tet-Li states, facilitating the SIT. In the MD simulations, the *Pnma* phase exhibits SIT at a lower T_c of 380 K (Figure 4e) than the original $P\bar{3}m1$ phase. The narrowed energy gaps in Li DOAS also lead to lower energy barriers for Li-ion migration, in agreement with the lower activation energy in the *Pnma* phase than in the $P\bar{3}m1$ phase. The lower diffusion barrier and lower T_c lead to a higher RT ionic conductivity.[20]

For the other SIC design strategy, mixed-anion substitution is induced to create diverse local anion-coordination of Li sites, which are broadened to a large number of Li states (Figure 4c). A candidate SIC trigonal $Li_3YBr_{1.5}Cl_{4.5}$ (LYBC) is created by randomly substituting 25 % of Cl with Br in $P\bar{3}m1$-LYC, and as a result, Oct-Li states have a variety of mixed Cl/Br anion-coordination with a close range of energy levels as observed in the Li DOAS (Figure 4i and S14). A large fraction of broadened Oct-Li states has narrowed energy gaps with Tet-Li states, facilitating the activations to disordered states of a SIC and leading to lower diffusion barriers. As a result, mixed-anion LYBC has a lower SIT T_c of 360 K and a higher Li ionic conductivity of 0.35 mS cm^{-1} at RT (Figure 4f) compared to 425 K and 0.02 mS cm^{-1}, respectively, in LYC (Figure 4d).

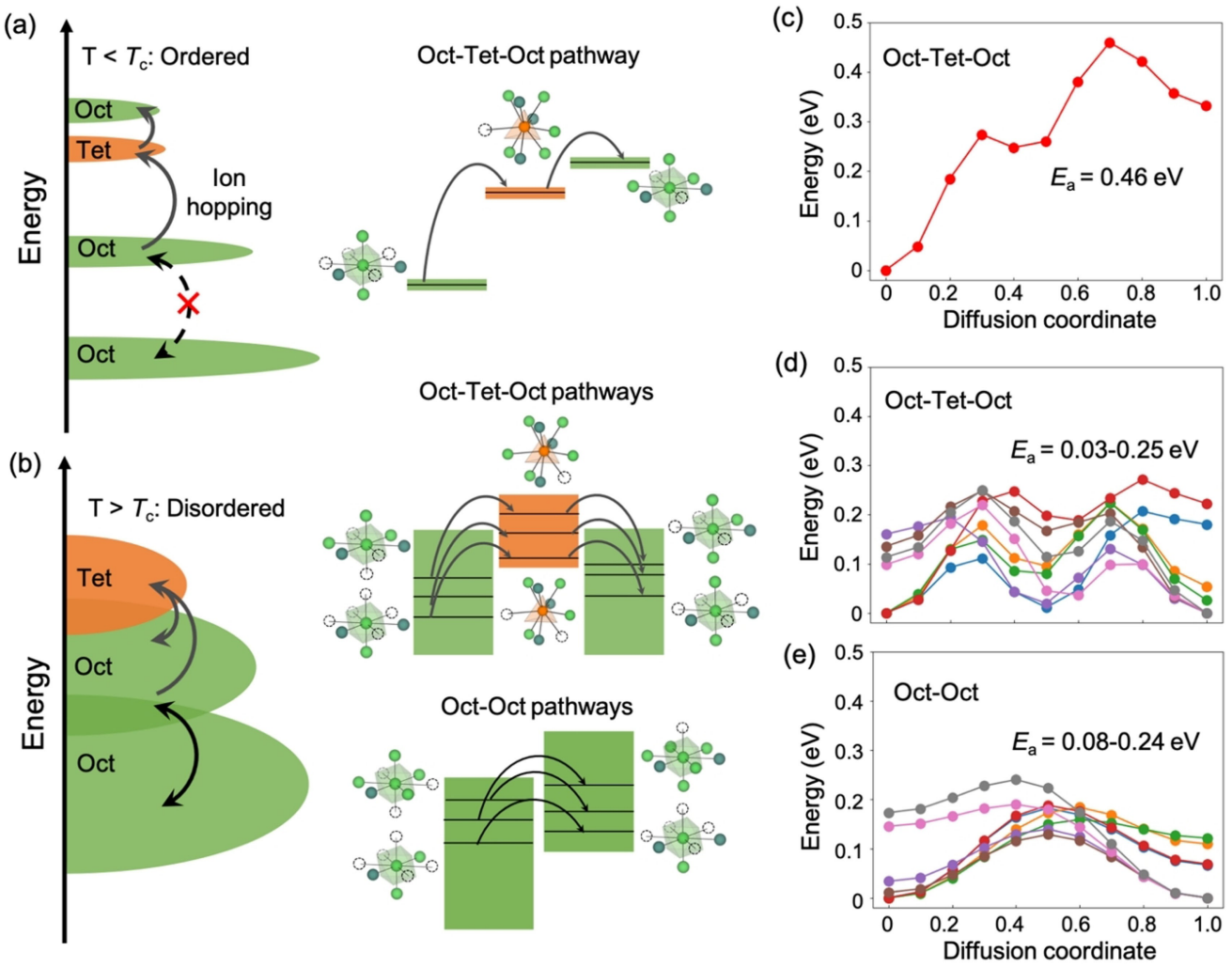

Figure 3. Diffusion mechanism before and after frustration. a), b) Schematic illustration of Li-ion migration (right) and corresponding state transitions in the Li DOAS (left) a) before and b) after the SIT. c)–e) The energy profile calculated by NEB methods for representative Li-ion migrations in c) ordered and d), e) disordered Li^+ sublattice of LYC.

The SIC design strategies can be generalized to other means that broaden mobile-ion states or introduce higher-energy states. For example, the modification of cation or anion sublattices can be achieved by high-entropy mixing of multiple cation or anion elements, which may cause extensive broadening of mobile-ion states for designing SICs.[21] The DOAS can be generally applied to unravel other types of frustration mechanisms, including distorted sites, geometric symmetry, and anion rotation, in other SICs.[10] As revealed by computational studies in known Li SICs,[10a,b,f,g] the crystal structure frameworks of SICs feature mobile-ion sites that are enlarged or distorted. These enlarged sites allow multiple positions for mobile-ion occupancy, thus broadening the mobile-ion states,[10f,g] and the distortion of the mobile-ion sites increases the site energies for the mobile-ions.[10b,c] Correspondingly, the materials design strategies that enlarge and distort mobile-ion sites have successfully designed new SICs.[10a,c,f,g,11a,22] Therefore, our DOAS provides a unified physics picture for a range of frustration mechanisms across many SIC materials and for the design strategies of new SICs.

Conclusion

In this work, we propose the analytics of the DOAS and demonstrate it in effectively unraveling the disordering mechanisms in atomistic systems, such as the SIT and frustration of mobile-ion sublattice in SIC. The evaluation of atomistic DOAS is straightforward using most MLPs, which provide atomistic energies of individual atoms by fitting the total lattice energies from DFT calculations. As demonstrated by studying the SIT in SICs, the DOAS has unique strengths in illustrating and understanding the mechanisms of frustration and disordering as follows.

1) The DOAS quantitatively characterizes the onset and degree of disordering by elucidating the energy distributions of local atomic states. For example, during an SIT, the frustration and disordering of mobile-ion sublattice

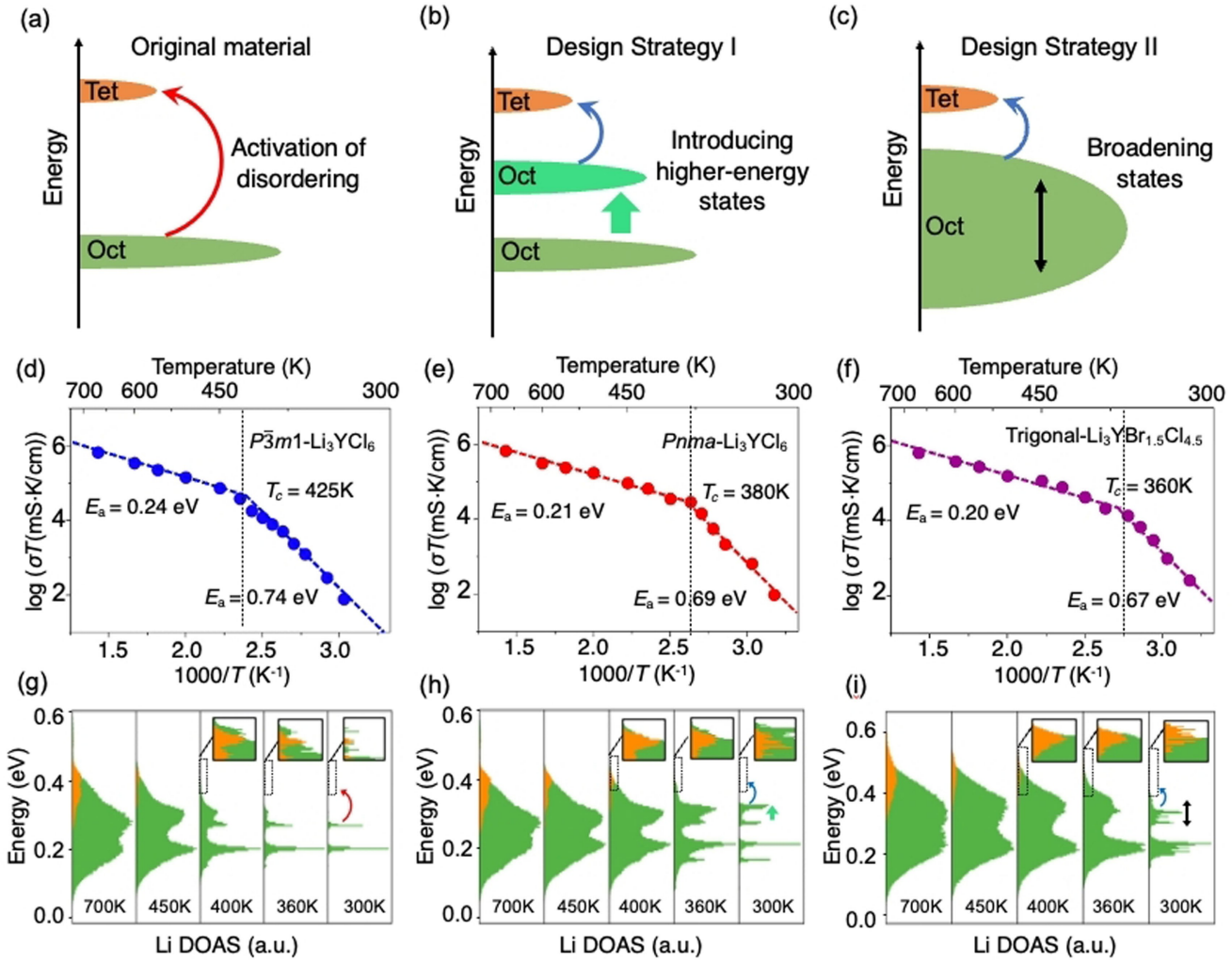

Figure 4. SIC design strategies guided by the DOAS. a)–c) Schematic DOAS illustrating SIC design strategies through (b) introducing higher-energy states and (c) broadening states. d)–f) The Arrhenius plot of Li^+ conductivity in d) $P\bar{3}m1$-Li_3YCl_6, e) *Pnma*-Li_3YCl_6, f) trigonal $Li_3YBr_{1.5}Cl_{4.5}$, and g)–i) corresponding Li DOAS at different temperatures.

correspond to a large number of locally disordered atomistic configurations with similar energy levels, which are characterized by the broadening of atomic states in the DOAS (Figure 2).

2) The energies and atomic configurations of states shown by the DOAS reveal the atomistic mechanisms that cause frustration and disordering. For example, as revealed by the Li DOAS, the SIT in LYC involves the activation of Tet-Li sites and locally disordered Oct-Li configurations (Figure 2), and the SIT in $Li_3YBr_{1.5}Cl_{4.5}$ is facilitated by the high-energy states of Li with mixed-anion coordination (Figure 4).
3) The DOAS effectively elucidates the transitions among states and their barriers in disordered materials. For example, fast ion diffusion in the frustrated ion sublattice of SICs is elucidated by the DOAS as the transitions among the broadened energy states of mobile ions with narrowed energy gaps (Figure 3, 4).

Our proposed DOAS is quantitative analytics and characterization that are generally applicable to disordering mechanisms. Other atomistic level mechanisms causing frustration such as dynamical bonding and anion rotational disorder in other SICs,[10b,d] can also be elucidated and analyzed by the DOAS. Furthermore, the DOAS can be further generalized and utilized for a wide range of phenomena, including glass transitions,[23] phase transitions,[24] nucleation and growth,[25] and complex fluid systems,[26] in which locally disordered atomistic configurations and energetics play crucial roles in the physical processes.[13] In addition to gaining insight and understanding, the DOAS can be used to guide the rational design of new SIC materials, as demonstrated in this study. Furthermore, our study illustrates a promising opportunity of combining atomistic modeling and ML techniques to extend and empower conventional physical analyses for unraveling fundamental mechanisms and guiding materials design.

Author Contributions

Y.M. and S.W. conceived the project. S.W. and Y.M. designed the computation and analyses. S.W. performed the computation and analyses. Y.M. and S.W. wrote the manuscript. All authors contributed to the interpretation of the results and the revision of the manuscript.

Acknowledgements

We acknowledge the funding support from National Science Foundation Award# 1940166 and the Cooperative Agreement (CA) Number W911NF-20-2-0284 and W911NF-22-2-0021. The views and conclusions contained in this document are those of the authors and should not be interpreted as representing the official policies of the U.S. Government. We acknowledge the computational facilities from the University of Maryland supercomputing resources and the Maryland Advanced Research Computing Center (MARCC).

Conflict of Interest

The authors declare no conflict of interest.

Data Availability Statement

The trained DP models and training data are available at https://doi.org/10.6084/m9.figshare.21822225.v1.

Keywords: Density of States · Disordering · Frustration · Ion Conductor · Machine Learning

[1] H. Zhao, J. Zhang, M. Lyu, S. Bachus, Y. Tokiwa, P. Gegenwart, S. Zhang, J. Cheng, Y.-f. Yang, G. Chen, *Nat. Phys.* **2019**, *15*, 1261–1266.

[2] X. Fabrèges, S. Petit, I. Mirebeau, S. Pailhès, L. Pinsard, A. Forget, M. T. Fernandez-Diaz, F. Porcher, *Phys. Rev. Lett.* **2009**, *103*, 67204.

[3] J. Snyder, J. S. Slusky, R. J. Cava, P. Schiffer, *Nature* **2001**, *413*, 48–51.

[4] S. M. Giampaolo, G. Gualdi, A. Monras, F. Illuminati, *Phys. Rev. Lett.* **2011**, *107*, 260602.

[5] a) J. Janek, W. G. Zeier, *Nat. Energy* **2016**, *1*, 16141–16144; b) N. Kamaya, K. Homma, Y. Yamakawa, M. Hirayama, R. Kanno, M. Yonemura, T. Kamiyama, Y. Kato, S. Hama, K. Kawamoto, A. Mitsui, *Nat. Mater.* **2011**, *10*, 682–686; c) Y. Zhou, X. Guan, H. Zhou, K. Ramadoss, S. Adam, H. Liu, S. Lee, J. Shi, M. Tsuchiya, D. D. Fong, *Nature* **2016**, *534*, 231–234; d) L. Q. Zhu, C. J. Wan, L. Q. Guo, Y. Shi, Q. Wan, *Nat. Commun.* **2014**, *5*, 3158.

[6] a) Y. Seino, T. Ota, K. Takada, A. Hayashi, M. Tatsumisago, *Energy Environ. Sci.* **2014**, *7*, 627–631; b) H. Yamane, M. Shibata, Y. Shimane, T. Junke, Y. Seino, S. Adams, K. Minami, A. Hayashi, M. Tatsumisago, *Solid State Ionics* **2007**, *178*, 1163–1167.

[7] H. J. Deiseroth, S. T. Kong, H. Eckert, J. Vannahme, C. Reiner, T. Zaiß, M. Schlosser, *Angew. Chem. Int. Ed.* **2008**, *47*, 755–758; *Angew. Chem.* **2008**, *120*, 767–770.

[8] H. Aono, E. Sugimoto, Y. Sadaoka, N. Imanaka, G. y. Adachi, *J. Electrochem. Soc.* **1990**, *137*, 1023.

[9] R. Murugan, V. Thangadurai, W. Weppner, *Angew. Chem. Int. Ed.* **2007**, *46*, 7778–7781; *Angew. Chem.* **2007**, *119*, 7925–7928.

[10] a) D. Di Stefano, A. Miglio, K. Robeyns, Y. Filinchuk, M. Lechartier, A. Senyshyn, H. Ishida, S. Spannenberger, D. Prutsch, S. Lunghammer, *Chem* **2019**, *5*, 2450–2460; b) N. Adelstein, B. C. Wood, *Chem. Mater.* **2016**, *28*, 7218–7231; c) K. Jun, Y. Sun, Y. Xiao, Y. Zeng, R. Kim, H. Kim, L. J. Miara, D. Im, Y. Wang, G. Ceder, *Nat. Mater.* **2022**, *21*, 924; d) Z. Zhang, H. Li, K. Kaup, L. Zhou, P.-N. Roy, L. F. Nazar, *Matter* **2020**, *2*, 1667–1684; e) B. Kozinsky, S. A. Akhade, P. Hirel, A. Hashibon, C. Elsässer, P. Mehta, A. Logeat, U. Eisele, *Phys. Rev. Lett.* **2016**, *116*, 55901; f) X. He, Y. Zhu, Y. Mo, *Nat. Commun.* **2017**, *8*, 15893; g) X. He, Q. Bai, Y. Liu, A. M. Nolan, C. Ling, Y. Mo, *Adv. Energy Mater.* **2019**, *9*, 1902078.

[11] a) Y. Zhang, X. He, Z. Chen, Q. Bai, A. M. Nolan, C. A. Roberts, D. Banerjee, T. Matsunaga, Y. Mo, C. Ling, *Nat. Commun.* **2019**, *10*, 5260; b) B. C. Wood, J. B. Varley, K. E. Kweon, P. Shea, A. T. Hall, A. Grieder, M. Ward, V. P. Aguirre, D. Rigling, E. Lopez Ventura, *Philos. Trans. R. Soc. London Ser. A* **2021**, *379*, 20190467.

[12] a) L. Zhang, J. Han, H. Wang, R. Car, E. Weinan, *Phys. Rev. Lett.* **2018**, *120*, 143001; b) S. Chmiela, A. Tkatchenko, H. E. Sauceda, I. Poltavsky, K. T. Schütt, K.-R. Müller, *Sci. Adv.* **2017**, *3*, e1603015; c) J. Behler, M. Parrinello, *Phys. Rev. Lett.* **2007**, *98*, 146401; d) A. P. Bartók, R. Kondor, G. Csányi, *Phys. Rev. B* **2013**, *87*, 184115; e) A. V. Shapeev, *Multiscale Model. Simul.* **2016**, *14*, 1153–1173; f) J. Behler, *J. Chem. Phys.* **2016**, *145*, 170901–170901.

[13] a) V. L. Deringer, C. J. Pickard, G. Csányi, *Phys. Rev. Lett.* **2018**, *120*, 156001; b) N. Bernstein, B. Bhattarai, G. Csányi, D. A. Drabold, S. R. Elliott, V. L. Deringer, *Angew. Chem. Int. Ed.* **2019**, *58*, 7057–7061; *Angew. Chem.* **2019**, *131*, 7131–7135.

[14] a) S. Wang, Q. Bai, A. M. Nolan, Y. Liu, S. Gong, Q. Sun, Y. Mo, *Angew. Chem. Int. Ed.* **2019**, *58*, 8039–8043; *Angew. Chem.* **2019**, *131*, 8123–8127; b) T. Asano, A. Sakai, S. Ouchi, M. Sakaida, A. Miyazaki, S. Hasegawa, *Adv. Mater.* **2018**, *30*, 1803075.

[15] Y. Zhang, H. Wang, W. Chen, J. Zeng, L. Zhang, H. Wang, E. Weinan, *Comput. Phys. Commun.* **2020**, *253*, 107206.

[16] X. He, Y. Zhu, A. Epstein, Y. Mo, *npj Comput. Mater.* **2018**, *4*, 18.

[17] H. Ito, K. Shitara, Y. Wang, K. Fujii, M. Yashima, Y. Goto, C. Moriyoshi, N. C. Rosero-Navarro, A. Miura, K. Tadanaga, *Adv. Sci.* **2021**, *8*, 21014133.

[18] J. Qi, S. Banerjee, Y. Zuo, C. Chen, Z. Zhu, M. L. H. Chandrappa, X. Li, S. P. Ong, *Mater. Today Phys.* **2021**, *21*, 100463.

[19] A. Bohnsack, F. Stenzel, A. Zajonc, G. Balzer, M. S. Wickleder, G. Meyer, *Z. Anorg. Allg. Chem.* **1997**, *623*, 1067–1073.

[20] J. Liang, E. van der Maas, J. Luo, X. Li, N. Chen, K. R. Adair, W. Li, J. Li, Y. Hu, J. Liu, L. Zhang, S. Zhao, S. Lu, J. Wang, H. Huang, W. Zhao, S. Parnell, R. I. Smith, S. Ganapathy, M. Wagemaker, X. Sun, *Adv. Energy Mater.* **2022**, *12*, 2103921.

[21] a) B. Helm, N. Minafra, B. r. Wankmiller, M. T. Agne, C. Li, A. Senyshyn, M. R. Hansen, W. G. Zeier, *Chem. Mater.* **2022**, *34*, 5558; b) F. Strauss, J. Lin, M. Duffiet, K. Wang, T. Zinkevich, A.-L. Hansen, S. Indris, T. Brezesinski, *ACS Mater. Lett.* **2022**, *4*, 418–423.

[22] S. Xiong, X. He, A. Han, Z. Liu, Z. Ren, B. McElhenny, A. M. Nolan, S. Chen, Y. Mo, H. Chen, *Adv. Energy Mater.* **2019**, *9*, 1803821.
[23] V. L. Deringer, N. Bernstein, G. Csányi, C. Ben Mahmoud, M. Ceriotti, M. Wilson, D. A. Drabold, S. R. Elliott, *Nature* **2021**, *589*, 59–64.
[24] R. Z. Khaliullin, H. Eshet, T. D. Kühne, J. Behler, M. Parrinello, *Nat. Mater.* **2011**, *10*, 693–697.
[25] a) J. Zhou, Y. Yang, Y. Yang, D. S. Kim, A. Yuan, X. Tian, C. Ophus, F. Sun, A. K. Schmid, M. Nathanson, H. Heinz, Q. An, H. Zeng, P. Ercius, J. Miao, *Nature* **2019**, *570*, 500–503; b) H. Chen, M. Li, Z. Lu, X. Wang, J. Yang, Z. Wang, F. Zhang, C. Gu, W. Zhang, Y. Sun, J. Sun, W. Zhu, X. Guo, *Nat. Commun.* **2019**, *10*, 3872.
[26] A. Neophytou, D. Chakrabarti, F. Sciortino, *Nat. Phys.* **2022**, *18*, 1248.

Manuscript received: October 21, 2022
Accepted manuscript online: February 7, 2023
Version of record online: February 23, 2023